Assessment of GHBMC M50-P Response for Behind Armour Blunt Trauma – Impact Loading with Approximation of 3D Surface of the Armour Back Face Displacement

Marcin Jenerowicz, Patrick Matt, Matthias Boljen, Steffen Bauer, Elmar Straßburger,
Stefan Hiermaier

Abstract The present study investigates numerically the assessment capability of the GHBMC M50-P with regard to behind armour blunt trauma (BABT) by applying impact loading with approximation of 3D surface of the armour back face displacement (BFD). The body armour consists of a hard-ballistic plate (9 mm silicon carbide and 10 mm ultrahigh molecular weight polyethylene, UHMW-PE) and a soft-ballistic component consisting of a 40-layer aramid fabric vest. The finite element model of the ballistic vest was applied to the GHBMC M50-P thorax using a novel forming simulation. A load case from previous experiments was selected where no penetration of the plate occurred (7.62 mm x 51 armour piercing projectile). For the approximation of the 3D surface of the BFD, the last layer of UHMW-PE at its maximum deformation was transferred from Ansys-Autodyn into LS-DYNA. For the evaluation of the BABT, the Viscous Criterion, the Blunt Criterion and the maximum strains in the impact area were used. The evaluation was performed at two locations: mid sternum ribs levels 3-4 and rib bone cartilage junction area at level 4. In both cases, the obtained probability of AIS2-3 injury was exceeded and the maximum strains indicate multiple fractures of the ribs or sternum.

Keywords Back Face Displacement (BFD), Behind Armour Blunt Trauma (BABT), Finite Element Simulation, Human Body Models (HBM), Injury Criteria

I. INTRODUCTION

Injury of the human body as a result of non-perforating ballistic impact into the personal protection equipment is defined as behind armour blunt trauma (BABT) [1]. Body armour protects law enforcement and military personnel from the severe effects of highly dynamic loads by dissipating kinetic energy of a projectile during impact. These highly dynamic loads can cause superficial contusion, soft tissue rupture, rib fracture, pulmonary contusion, and cardiac injuries depending on the impact location [2]. The velocity of the back face of the deforming armour exhibits a rapid rise to a maximum acceleration within a few microseconds followed by a drastic decrease until the back face deformation (BFD) has reached the maximum, which depends on the projectile type and velocity, as well as the structure of the body armour [3]. The United States Department of Justice (DOJ) described a static 44 mm maximum BFD as the pass/fail threshold for ballistic armour certification, which provides a baseline metric for comparing armour effectiveness with regard to BFD [4, 5]. A homogenous block of nonhardening, oil-based modelling clay is placed in contact with the back of the armour panel during ballistic testing, which is used as a body substitute mass. The decisive criteria that led to the use of modelling clay were not based on the supposed similarity to the deformation behaviour of human tissue, but on the very good and inexpensive repeatability of the experiments and the easy access to retrospective measurements, due to the good plastic deformability. For this reason, the 44 mm referred to does not concern the maximum deformability of the protective material, but the permanent deformation of the clay. Unfortunately, the remaining deformation in the clay does not provide information about the actual dynamics of the BFD that cause the type and severity of potential injuries. This forms the critical component for replicating ballistic events in a simulated environment.

Finite-element (FE) human body models (HBM) are used to a great extent for crash and impact simulations in the automotive industry [6–10]. However, despite the fact that HBMs have been validated for a wide range of crash loading cases, their use in defence applications to study ballistic threats to the human body tends to be limited to non-lethal kinetic projectiles and blunt impacts [11–13]. One of the reasons is the difficulty of modelling

M. Jenerowicz (e-mail: marcin.jenerowicz@emi.fraunhofer.de, tel: +49-761-2714-359) is a Research Fellow at the Fraunhofer Institute for High-Speed Dynamics, Ernst-Mach-Institute (EMI), and a PhD candidate at the Faculty of Engineering of the Albert-Ludwigs-University in Freiburg, Germany. S. Hiermaier is Professor for Sustainable Systems Engineering at the Faculty of Engineering of the Albert-Ludwigs-University and the Director of the Fraunhofer Institute for High-Speed Dynamics, EMI. P. Matt, M. Boljen, S. Bauer, and E. Straßburger are affiliated with the Fraunhofer Institute for High-Speed Dynamics, EMI, Germany.

flexible clothing, as well as protective components in worn form, directly on the human body. The ballistic protection components of most of these systems consist of a deformable soft ballistic package that conforms to the carrier and a hard-ballistic plate that intercepts the primary impact of the projectile which, in the best case, shatters it. The soft ballistic package is intended to act as a second layer of protection, whereby both components are essential for the efficiency against projectiles and interact together. Even if the hard-ballistic plate is penetrated and appear to fail, it still fragments the projectile and decelerate all particles so that the soft ballistics can absorb the remaining kinetic energy and stop the shrapnel cloud. Although many constitutive models for fabric materials are available for various applications [14–16], few attempts have been made to use them directly in clothing models on HBMs. A modelling technique has been developed to drag simple fabric components from a 2D shape into the 3D shape defined by the body surface of the subject wearing the fabric [17]. This method resembles a deep drawing process that uses a dynamically evolving stamp geometry to continuously restore the original body surface after previously reducing it to a planar surface (Fig. 1). The technique provides a simple way to drape flexible objects onto arbitrary contours. More complex garments, e.g. long-sleeved shirts, cannot be captured using this approach, especially if they have to be combined with various HBM postures. However, the proposed method can be modified and alternatively applied by pressing a flexible, flat object inversely onto the HBM contour from the outside. In a later study, this method has been investigated for a multilayer fabric package of a soft ballistic armour [18]. In the present study, the assessment capability of the GHBMC M50 is investigated in relation to BABT for a projectile impact on a hard-ballistic plate with soft ballistic material located behind it.

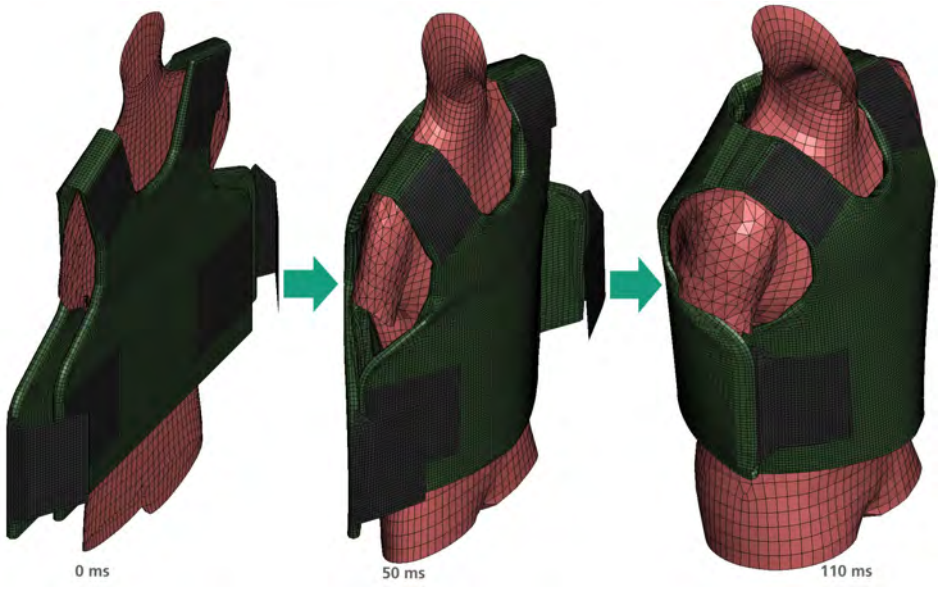

Fig. 1. Forming process of a finite element vest model from 2D planar to 3D donned shape with the body contour of the GHBMC M50 expanding from the interior of the vest [17].

II. METHODS

FE Model Development

The ballistic impact of a 7.62 mm × 51 AP8 projectile on a hard-ballistic plate made of 9 mm silicon carbide (SiC) and 10 mm of an ultra-high-molecular-weight polyethylene (UHMW-PE) component forms the baseline of the following investigation. The penetration resistance of the hard-ballistic plate was validated experimentally and numerically in Ansys-Autodyn [19]. From this study, a load case was selected for the present BABT investigation in which no penetration of the hard-ballistic plate occurred. Figure 2 (a) shows the hard-ballistic plate (9 mm SiC, 10 mm UHMW-PE) after an impact with the AP8 projectile at $v_P = 913$ m/s with the remaining buckling. The maximum dynamic BFD during the experiment is much larger (maximum displacement 23.2 mm) than the remaining BFD in Figure 2 (a). This is due to the relaxation of the material after the impact. A displacement-time profile was recorded with a high-speed camera (frame rate: 125 kHz). Figure 2 (b) shows the corresponding simulation of the performed experiment with Ansys-Autodyn. In the simulation, the target is not fixed at the edges and the projectile is also not completely fragmented. At the time shown (t = 0.15 ms), the deceleration

process was almost complete, but the projectile and the layers were still moving with a constant residual velocity of approximately 94 m/s. Since the layers were not penetrated any further, this was evaluated as 'target has resisted, no full perforation'.

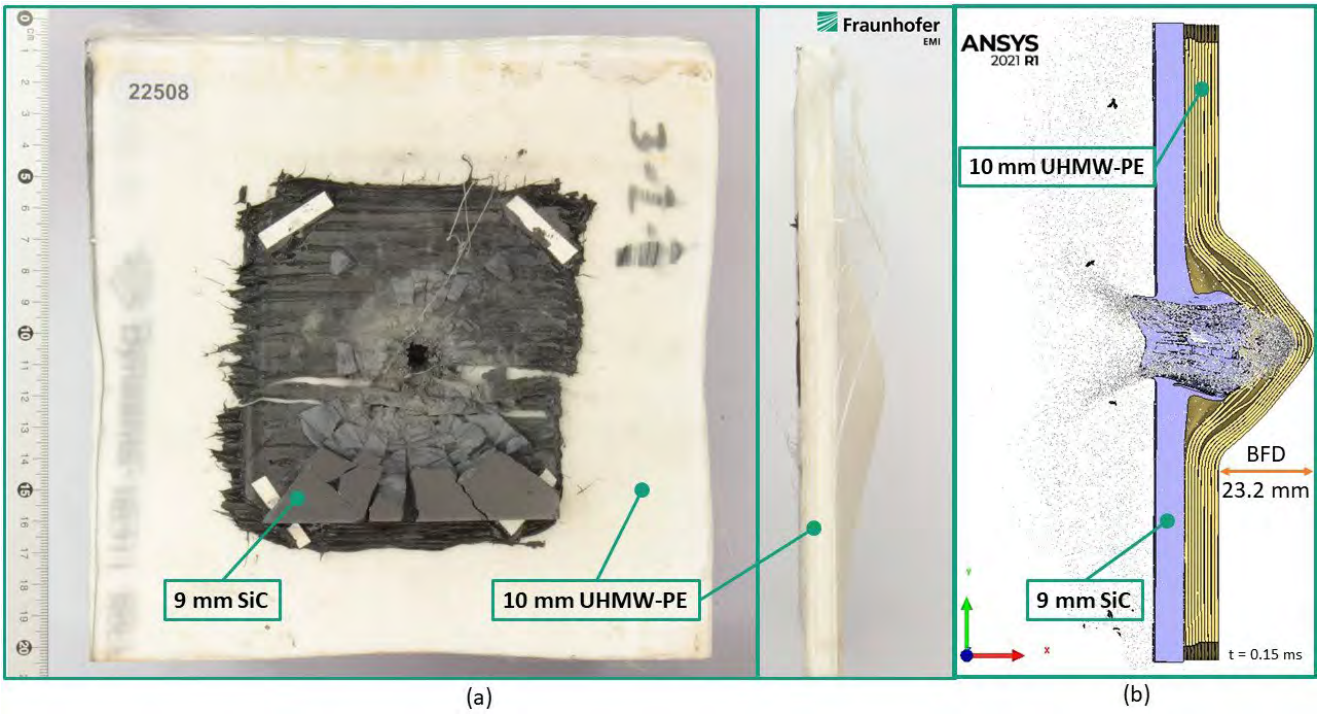

Fig. 2. (a) Hard-ballistic plate of 9 mm silicon carbide (SiC) and 10 mm of an ultra-high-molecular-weight polyethylene (UHMW-PE) after impact with 7.62 mm x 51 AP8-Projectile at $v_P = 913$ m/s); (b) corresponding simulation of the performed experiment with Ansys-Autodyn, maximum back face deformation (BFD) 23.2 mm at 0.15 ms.

The maximum BFD encountered in the Ansys-Autodyn simulation is transferred to a soft ballistic package in LS-Dyna. The transfer to another finite element environment is necessary due to the requirement of additional, specific and expensive licences for the material reproduction of the UHMW-PE in LS-Dyna. Furthermore, the application of the used HBM is limited to LS-Dyna. The soft ballistics consists of three fabric packages containing 13, 14 and 13 individual plies, respectively. The plies are oriented alternately in the 0°/90° and ±45° orientations, with each ply having a thickness of 0.28 mm. The plies are sewn together along the perimeter of each package. A simplified model of the soft ballistics was implemented in order not to increase the computational time excessively. In this model, six, seven and six element layers are represented for the individual fabric packages. Each element layer consists of two integration points in the thickness direction, each of which represents a real physical fabric layer. Therefore, a total of 38 fabric layers are mapped. The division into 3 packages is not represented numerically. The material parameters for the analysis in LS-Dyna were taken from Ivanov and Tabiei [14]. For the forming algorithm, only the innermost layer of the entire vest was subjected and after forming, subsequently stacked to the actual number of layers. Following draping, the individual plies were packed via boundary conditions to form the stitched package of 38 layers. The virtual stamp was generated by an upscaled duplicate of the GHBMC M50-P (v.5-3-3) body surface representing a 50th percentile male (height 175 cm, weight 77.28 kg), which was used for the analysis of the present study. Figure 3 shows the formation of the soft ballistic layer used for this study that was applied to the GHBMC M50-P contour model. A slot of about 350 mm was created between the outer punch and the body surface, in which the non-deformed fabric layer was located. The material points of the punch were then relocated back to almost the original position on the body surface. The fabric layer, consisting of about 12,500 four-sided shell elements, was thereby forced into the shape of the body surface [18].

(a) (b) (c) (d)

Fig. 3. (a) Setup for forming the innermost fabric layer on GHBMC M50; Intermediate configurations after completion of (b) 60 %; (c) 80 % and (d) 95 % displacement [18].

For the approximation of the 3D surface of the BFD, the deformation history of the BFD is used to specify the displacement and shape of the substitute impactor layer (SIL). The node set with corresponding relative positions of the last posterior layer of UHMW-PE hard-ballistic structure was extracted for 5 points in time until the maximum deformation is reached (*t* = 0.15 ms) from Ansys Autodyn, which describes the evolving geometry of the BFD. The node set positions were assigned to a SIL in LS-Dyna, which imprints itself into the soft ballistic layers as a rigid part with fixed displacement-time boundary conditions. In this case, the soft ballistic has no decelerating effect on the SIL and no momentum transfer occurs. Nevertheless, the real ballistic BFD was applied, which realises impact deformation transferred into the fabric package and into the GHBMC M50-P.

For further evaluation of the BABT and the impulse transfer to the GHBMC M50-P, the impulses of all nodes from all positions of the hard-ballistic plate and the projectile were determined, which transmitted the total impulse to the soft ballistic. The following was considered for this setting: the nodes were assigned to different rings based on their radial position relative to the impact centre, which were constantly expanded in a 5 mm radius, i.e. all nodes with radial distance smaller than 5 mm to the impact axis were located in the innermost ring, all nodes with radial distance between 5 and 10 mm were located in the second ring, and so on. For each ring, the mass of all contained nodes and the total momentum in the direction of the shock (Fig. 2 (b), *x*-axis) were then determined. Only nodes that had a positive velocity (v_x) were considered. This prevented nodes ejected from the annulus (- v_x) from reducing the total momentum. The total mass and total *x*-momentum were then calculated for each ring, and $p = m \cdot v$ was used to calculate the total velocity of the ring in each case. In addition to the condition that v_x must be positive, it is required that the relevant nodes must be to the right of the original target backside (nodes inside the buckling), i.e., in the region of influence acting on the soft-ballistic package. The effect up to the outermost ring of the SIL (radius 35mm) was considered. Beyond that, the impulses were negligibly small. This results in $\overline{m}_{SIL} = 41$ g and $\overline{v}_{SIL} = 113.4$ m/s for the momentum at t = 0.15 ms.

The SIL was applied at two specific areas for the present study. Point of interest (POI)-1 is located directly over the midline of the sternum, mid between 3rd-4th ribs and POI-2 at the sternal end of the 4th rib at the junction between cortical bone and the costal cartilage. Figure 4 (a) shows the applied SIL deformation at POI-1 and Fig. 4 (b) at POI-2 on the GHBMC M50-P at t = 0.15 ms.

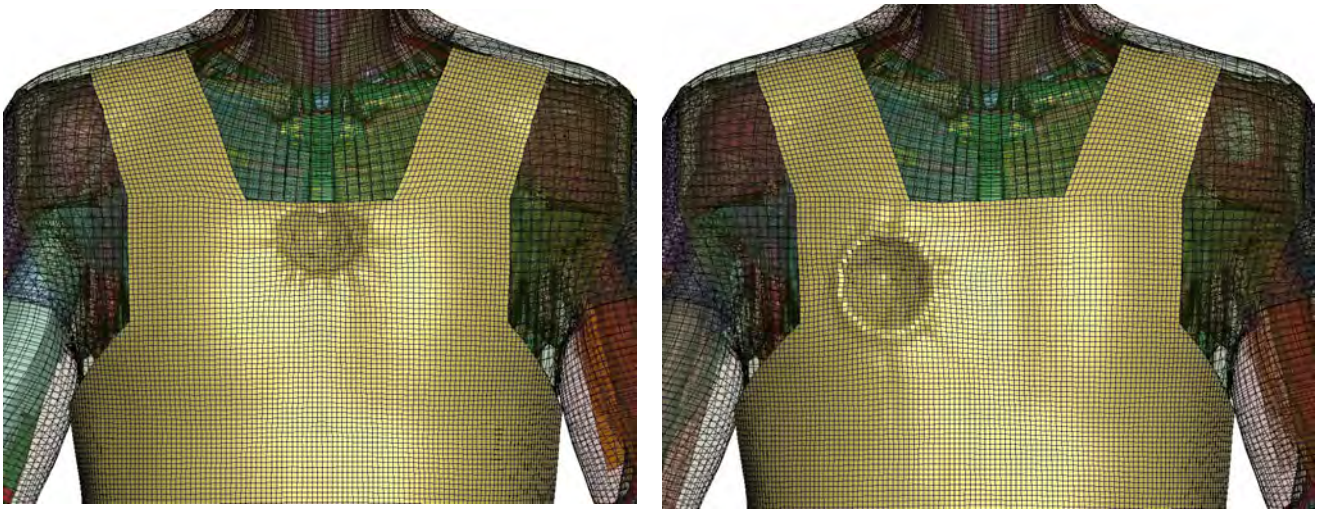

(a) (b)

Fig. 4. Soft ballistic armour deformation by substitute impact layer (SIL) on the GHBMC-M50-P at t = 0.15 ms: (a) at impact location POI-1; (b) at impact location POI-2.

Assessment of BABT (Injury Criteria)

One model for assessment of BABT is based on research conducted by Clare et al. in the 1970s [20] which has evolved into a multi parameter model [21]. The *Blunt Criterion* (BC) is defined by the following equations:

$$BC = \ln\left(\frac{E_{kin}}{t_{BWT} \cdot d_P \cdot W^{1/3}}\right) \tag{1}$$

with $E_{kin} = \frac{1}{2} \cdot m_1 \cdot {v_1}^2$, and

$$E_{kin.,eff} = \frac{1}{2} \cdot m_1 \cdot {v_1}^2 - \frac{1}{2} \cdot (m_1 + m_2) \cdot {v_2}^2 = \frac{1}{2} \cdot m_1 \cdot {v_1}^2 \left(1 - \frac{m_1}{m_1+m_2}\right) \text{ for } v_2 = \frac{m_1 \cdot v_1}{m_1+m_2};\ v_2 \neq 0 \tag{2}$$

where t_{BWT} is the body wall thickness (BWT) of the individual in [cm], d_P is the diameter of the projectile in [cm], W is the mass of the individual (or struck target) in [kg], E_{kin} is the kinetic energy of the projectile at impact in [J] with m_1 as the mass of the projectile in [kg], and v_1 as the velocity of the projectile in [m/s]. In Equation (2), the conservation of momentum was used to estimate the effective energy $E_{kin.,eff}$ of the inelastic collision, where m_2 is the effective mass of the body part or existing body protection equipment struck in [kg], and v_2 is the velocity of the combined mass $(m_1 + m_2)$ in [m/s]. Since the transfer of impulse energy to the rest of the body is relatively slow in relation to the rate of injury on impact, the body mass affected is only the effective mass of the part of the torso that moves with the projectile on impact. The momentum of the projectile was obtained by the momentum of the combined mass of the body part or armour and the projectile after impact in Eq. (2) [21].

The approach to estimate the BWT was suggested by Sturdivan at al. [21] as following:

$$t_{BWT} = k \cdot W^{1/3} \tag{3}$$

where k is 0.711 for male and 0.593 for female subjects. Real thickness data from human subjects to calculate the parameter k was taken on the lateral rib cage directly over the ribs and the centre of the lung [21]. For the GHBMC M50-P with a total mass of 77.28 kg, the BWT is $t_{BWT} = 3.03$ cm. In [22], the BWT was measured with computer tomography scans for 23 adults and 17 children to demonstrate the difference in thickness of the thoraco-abdominal wall. The results showed that for children (< 16 years), penetrating injury of the same depth can more likely breach the body wall and potentially damage a greater number of organs. BWT was defined as the measurement taken from the epidermal surface to the interface of the hypodermis and underlying muscle [22]. Results for adult subjects at Manubrio-sternal angle are 2.5 cm and at the Xiphisternum 2.2 cm. Considering that the impact point (POI-1) is located in the middle of the sternum, the calculated value with k = 0.711 would

overestimate the average value of [22] by 17-27 %. The actual BWT of the GHBMC M50-P at the Xiphisternum is 1.91 cm and at mid-sternum 2.42 cm. For POI-2, the BWT of the GHBM-M50-P is 2.73 cm, which deviates only by 10 % from [21].

The second injury criterion considered in this study is the *Viscous Criterion* (VC) [23], which has been validated in-depth for motor vehicle occupants and some pertinent injury cases from ballistic impacts of post-mortem human subjects (PMHS) [24]. The VC describes the injury tolerance of soft tissue during the rapid phase of impact deformation of the body, or the viscous response and is defined by the following equation:

$$\mathrm{VC} = \mathrm{V(t)} \cdot \mathrm{C(t)} = \frac{d\mathrm{D(t)}}{d\mathrm{t}} \cdot \frac{\mathrm{D(t)}}{\mathrm{D_0}} \tag{4}$$

where D(t) is the chest deflection and $\mathrm{D_0}$ the initial chest depth (GHBMC M50-P: $\mathrm{D_0}$ = 230 mm). Analysis by Viano and Lau indicates that the combination of velocity and amount of compression ($\mathrm{V(t)} \cdot \mathrm{C(t)}$) has a higher predictive ability of injury than either velocity or amount of compression alone [23]. In addition, they validated the VC by examining existing PMHS data and it was outlined that the maximum viscous response highly corelates to the risk of severe soft tissue and internal organ injury. Bir and Viano [24] show for blunt ballistic impacts with three different conditions (impactor A: 140 g at 20 m/s, impactor B: 140 g at 40 m/s and impactor C: 40 g at 60 m/s) that each condition gives distinctive injury responses, which vary from those reported in the automotive literature for lower speed impacts [25]. This study indicates that further validation of the VC for the prediction of injuries from blunt ballistic impacts is required and any collected data from simulations used for comparison should be viewed with caution.

In the present study, the displacement-time data at the examined locations POI-1 and POI-2 was used to calculate the biomechanical parameter $\mathrm{VC_{max}}$. The calculation on the GHBMC M50-P for POI-1 was made under the assumption that the sternum moves uniformly. The analysis was done using the displacement-time data and the corresponding velocity for the centre of mass of the sternum. For POI-2, ten nodes were selected from the sternal end on the anterior side centrally along the length of the costal arch and also analysed for displacement-time data and corresponding velocities. The position and number of nodes chosen here form an average value that was used for the analysis. The maximum determined displacement varies greatly in relation to the relative distance to the sternal end. Depending on the number and position of the nodes, the value can vary considerably. The influence of these parameters on the VC and possibly the mesh size should be investigated in a further study. The results were combined with the injury data and rankings from literature [24]. In addition, the resulting maximum principal strains were determined and compared with data from the literature, which has the objective of exploring sources of variation in rib structural properties in order to identify sources of differential risk of rib fracture between vehicle occupants [26].

In order to have a comparable use case to the SIL, another event is used to calculate the BC. The primary case describes the transfer of the BFD through the SIL to the soft-ballistic package and the GHBMC M50-P based on the simulation results in LS-Dyna. The second case is a real instance that occurred during the investigation of the hard-ballistic plate by E. Straßburger et al. [19]. In this case, the AP8 projectile was partially stopped by the hard-ballistic plate, which was fixed in a frame without backing material. Only the fragmented projectile core pierced through the plate (tungsten carbide: $\mathrm{d_P} = 5.6\ \mathrm{mm}, \mathrm{m_{core}} = 5.9\ \mathrm{g}$) with the residual velocity of $\mathrm{V_R} = 103\ \mathrm{m/s}$. It is assumed that the remaining fragment impact is non-penetrative to the soft ballistic material. Currently, this aspect is still being investigated. This case presents different boundary conditions with ongoing examination, but will also serve as a comparison to the SIL simulation. For all defined load cases, the kinetic energies were calculated from Eq. (2), with the corresponding masses of the impactors $\mathrm{m_1}$ and the soft ballistic package $\mathrm{m_2} = 1.275\ \mathrm{kg}$. The AP8 core load case was not included in the calculation of the VC because the actual deformation caused by the BFD to a body protection user is currently unknown. This will be investigated in a further study.

III. RESULTS

Figure 5 shows the maximum principal strains occurring after application of the BFD with the SIL for (a) POI-1 and (b) POI-2 at t = 0.15 ms.

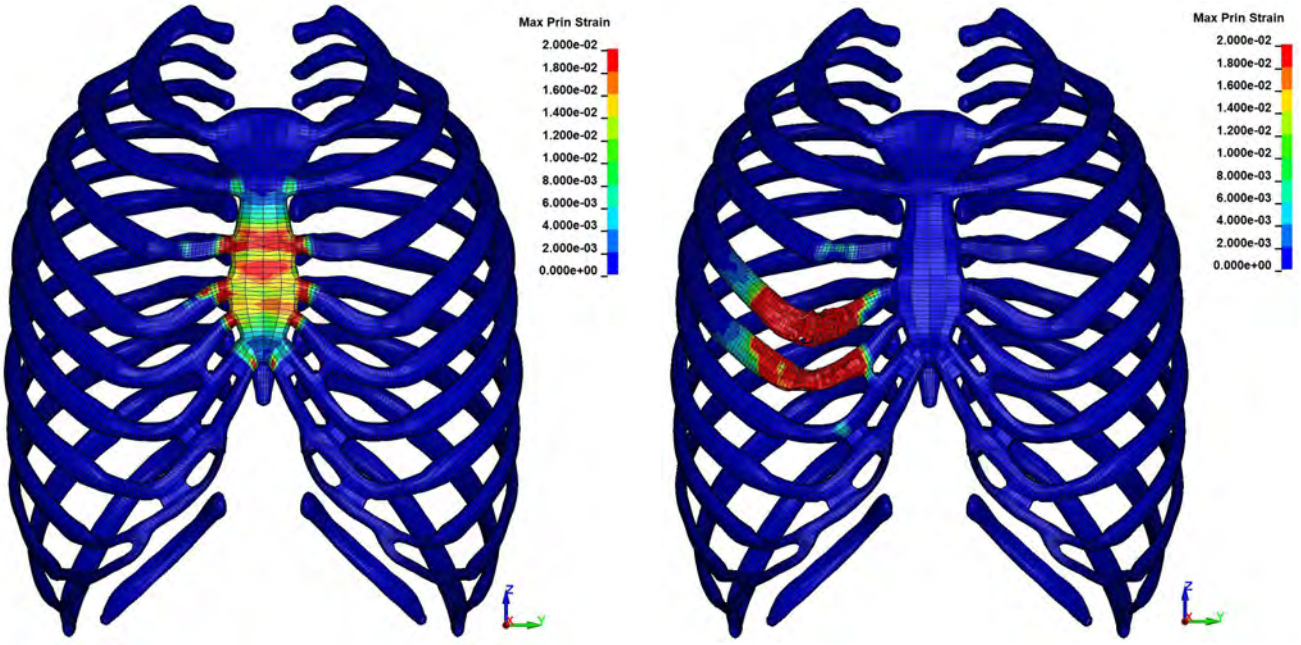

(a) (b)

Fig. 5. Plot of maximum strains occurring up to the 2 % limit according to [27] after BFD applied with SIL at t = 0.15 ms; (a) POI-1, (b) POI-2.

The scale of the maximum principal strain is set to the limit value of 2 %, as fractures and severe tissue damage can be expected from this value according to [27]. It is evident that the strains occurring in POI-1 are distributed almost symmetrically in the sternal region. The maximum values occur in the middle of the impact point and at the transition areas to the costal cartilage. The affected areas marked in red would reveal fractures exceeding thresholds set in GHBMC M50-P corresponding to [27]. In Figure 5 (b), the area of influence of the BFD through the applied SIL over the transition area from the sternal end of the 4th rib, has clearly transitioned to the 5th rib. The exceeded 2 % strain limit suggests that both ribs are fractured. As a note, it should be mentioned here that the limit set far exceeds that from the literature. According to [26], a much lower limit value for an M50 should be applied, namely 1.25 ± 0.25 %. This would make the range of injury even significantly larger.

Figure 6 shows the calculated VC progression and corresponding displacement and velocity in x-direction over time. For POI-1 at the sternum, the centre of mass (CoM) was compared to the average values of the whole FE sternum part. The displacements are relatively constant over time, and the velocities reach their maximum value relatively shortly after the impact and decrease steadily. For POI-2, the values increase relatively constantly, although a delay occurs at the beginning. This results from the position of the SIL, which is not completely orthogonal above the impact location. The SIL does not have a curved surface and a rotation would change the impact axis relative to the body surface. From about 0.12 ms, there are strong fluctuations in the velocity progression, which greatly depends on the position of the selected nodes for the evaluation. The closer to the sternal end, the greater the discrepancies, as edge effects at the transition to the cartilage tissue can influence the results significantly.

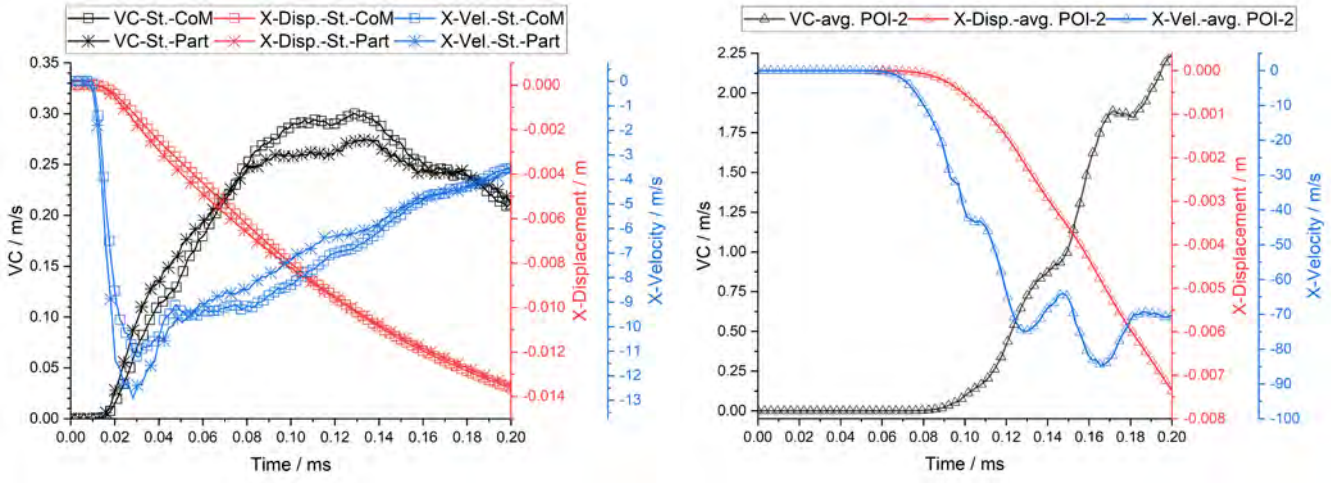

(a) POI-1 (b) POI-2

Fig. 6. Plot of calculated VC and corresponding displacement and velocity in impact x-direction over time at impact points: (a) POI-1 with comparison of different computation locations for the sternum; centre of mass (CoM) and whole part, (b) POI-2 with estimated average values of ten nodes selected from the sternal end on the anterior side centrally along the length of the costal arch.

All determined characteristic values and the comparative characteristic values according to [24] with comparable body weight to the M50 (except for impactor A, which were all defined as AIS 0) are summarised in Table I.

TABLE I

CALCULATED BC AND VC IN RELATION TO AIS INJURY PARAMETER ACCORDING TO [24] WITH COMPARABLE BODY WEIGHT (*BWT ACCORD. TO EQ. (3))

Impact Condition	Mass (kg)	Velocity (m/s)	Energy (J)	Diameter (cm)	Weight (kg)	BWT (cm)	BC (-)	VC_{max} (m/s)	AIS
*SIL-POI-1**	0.041	113.4	263.62	7.0	77.28	3.03	1.10	0.29	3
SIL-POI-1	0.041	113.4	263.62	7.0	77.28	2.42	1.33	0.29	3
SIL-POI-2	0.041	113.4	263.62	7.0	77.28	2.73	1.21	1.95	2
*AP8-POI-1**	0.0059	103.0	31.29	0.56	77.28	3.03	1.47	N.A.	2-3
AP8-POI-1	0.0059	103.0	31.29	0.56	77.28	2.42	1.70	N.A.	2-3
AP8-POI-2	0.0059	103.0	31.29	0.56	77.28	2.73	1.58	N.A.	2-3
B [24]	0.14	37.78	99.91	3.7	74	2.98	0.77	1.97	2
B [24]	0.14	40.87	116.93	3.7	82	3.09	0.86	2.35	2
B [24]	0.14	43.24	130.88	3.7	79	2.54	1.18	2.18	2
C [24]	0.03	63.24	60.45	3.7	79	2.54	0.4	0.59	0
C [24]	0.03	61.26	56.29	3.7	82	3.09	0.13	0.9	0

IV. DISCUSSION AND LIMITATIONS

Comparing only the kinetic energies of SIL and the AP8, it is clear that the influence of the BFD of the hard-ballistic plate should not be underestimated, although the energy transfer of the BFD is not determined in the penetration case. Also, an approximation of the photographed back side of the hard-ballistic plate to one in real contact with the body was made. The interaction between armour and torso may change the dynamic profile under deformation. The differences and validation of the experimental set-up should be further investigated. It should also be considered that the influence of the BFD is not included in the calculation of the BC. Although the BC characteristic values are relatively high and, according to [24], consistently suggest an AIS2-3 injury, it has to be taken into account that in the case of a projectile penetration, the area of influence to which the energy can dissipate is significantly smaller. Both publications [20, 21] of the BC development primarily address soft personal protective armour. The influence of BFD on hard-ballistic plates was not considered at the time. Since BC values cannot be encompassing for every type of body armour due to the limitations of the formulation, the feasibility of this method should be investigated in further validation tests.

The application of a suitable BWT is also important for the calculation of the BC. If no specific information exists, the approximation according to Eq. (3) is valid. Nevertheless, the direct measurement of the BWT is to be preferred, as the soft tissue thickness can vary greatly depending on the body region. This is also easily realised when using HBM.

The determined $\mathrm{VC}_{\max}$ values are also in strong contrast to the BC values. The determination of these is not trivial for HBM. For POI-1, a second reference value was determined describing the mean displacement of the entire sternum part. Here, a deviation of approx. 8.5 % occurred in comparison to the centre of mass of the sternum, whereby in the conclusion, the larger value was considered. The $\mathrm{VC}_{\max}$ at POI-2 is significantly larger, since the load and resulting velocity of the selected nodes for evaluation at the 4th rib are considerably larger than at the sternum. The position of the SIL is not completely orthogonal above the impact location, since the SIL does not have a curved surface. The rotation of the SIL would change the impact axis relative to the body surface. The development of a SIL aligned with the body shape depending on the impact location is the subject of further studies. The development of the VC is based on a relatively deformed thorax at much lower strain rates than in the present study. Here the opposite occurs, a locally slightly deformed thorax at very high strain rates, which makes the applicability of the VC difficult. The overall deformation of the thorax is usually marginal at the small impact areas and does not correlate with the injury patterns identified. The criterion was used for comparison since it has also been used in the literature for blast impacts [25]. Nevertheless, it should be noted that the validation base from PMHS trials is relatively small and should be expanded.

The elements of the rib cartilage erode at POI-2 if the deformations are too severe (invokes a failure criterion based on maximum principal strain equal to 1 %). This is a default setting in the GHBMC M50-P part costal cartilage whose influence on the overall deformation of the ribs needs to be investigated. This occurs in the calculation at POI-2, so these results should be revalidated in adjusted parameter studies. In addition, edge effects can occur that complicate the evaluation at the sternal end of the ribs. Furthermore, effects of nonphysical element erosion on the entire computational validity following the first erosion should be investigated. Element erosion is also provided for other parts of the GHBMC models, such as the cortical bone materials. As already mentioned, its threshold value is defined at 2 % of the maximum principal strain, but it is much easier to switch off than for the cartilage tissue. This is often used to avoid stability problems in calculations with high strain rates by deleting elements with strong short-term distortion. In small local cases, as in the presented study, this unfortunately leads to inconsistencies in the results. According to [26], the assumed threshold value of 2 % strain is far too high for an M50. It was shown that a value of (1.25 +/- 0.5) % would be preferable. Nevertheless, it should be noted that the tests were carried out at a rate of ~2 m/s, and it is not possible to conclusively clarify the behaviour at significantly higher strain rates. The basic applicability of the GHBMC M50-P model outside any validation of local details or structural material properties at strain rates implied by an entrance velocity above 100 m/s should be revised. Defined thresholds, which are largely unavailable for this strain rate range, need to be identified to prepare the model for validation analyses.

V. CONCLUSIONS

In the present study, a new method was introduced to transfer the BFD of a hard-ballistic plate realistically to an HBM (GHBMC M50-P) wearing a soft ballistic protective vest applied directly to the body by means of a forming simulation. Two impact points were defined: on the midline of the sternum centred between the 3rd and 4th ribs (POI-1), where the largest mean deformations of the thorax were expected and at the transition area of the 4th rib from the sternal end to the costal cartilage (POI-2), where the load on the rib was highest. For the evaluation of the BABT, the BC and $\mathrm{VC}_{\max}$ were compared and the maximum strains occurring in the thorax were presented. In all cases, an AIS2-3 rating can be assumed to be exceeded. However, the determined characteristic values must be considered critically. Certain limit values, defined in the GHBMC M50-P model originating from the automotive area, are calibrated for these load cases. For the very high dynamic and extensive loads occurring on a significantly smaller area of influence, which results from the small effective range of the projectile, the numerical model reaches its representable limits. For further investigations of the BABT on GHBMC models, it will be necessary to calibrate them for the new load cases and to validate them with comparisons from PMHS tests.

In general, an energy-based assessment criterion such as the BC is preferable to the VC, both being valid for specific use cases. An energy-based criterion can better describe the load case, which implies a highly dynamic loading scenario such as blast impact, on a local level. Nevertheless, the applicability has to be critically evaluated, and each case has to be assessed individually.

VI. ACKNOWLEDGEMENT

We would like to express our appreciation to the Federal Office of Bundeswehr Equipment, Information Technology and In-Service Support (BAAINBw, Koblenz, Germany) as well as Bundeswehr Technical Center for Weapons and Ammunition (WTD-91 GF-450, Meppen, Germany) and the Bundeswehr Defense Technology Center for Protection and Special Technology (WTD-52 GF-320, Oberjettenberg, Germany) for funding this work.

VII. REFERENCES

[1] Prather, Russell N. Swann, Conrad L. Hawkins, Clarence E. (1977) Backface Signatures of Soft Body Armors and the Associated Trauma Effects, The Defense Technical Information Center (DTIC).

[2] Lidén, E.; Berlin, R.; Janzon, B.; Schantz, B.; Seeman, T. (1988) Some observations relating to behind-body armour blunt trauma effects caused by ballistic impact. The Journal of trauma, **28** 1 Suppl: S145-8.

[3] Cronin, D. S.; Bustamante, M. C.; Barker, J.; Singh, D.; Rafaels, K. A.; Bir, C. A. (2021) Assessment of Thorax Finite Element Model Response for Behind Armor Blunt Trauma Impact Loading Using an Epidemiological Database. Journal of biomechanical engineering, **143** (3).

[4] Ballistic Resistant Protective Materials - NIJ Standard 0108.01 (1985), National Institute of Justice, [https://nij.ojp.gov/library/publications/ballistic-resistant-protective-materials-nij-standard-010801, 21.03.2023].

[5] Ballistic Resistance of Body Armor - NIJ Standard-0101.06 (2008), National Institute of Justice, [https://nij.ojp.gov/library/publications/ballistic-resistance-body-armor-nij-standard-010106, 21.03.2023].

[6] Gayzik, F. S.; Moreno, D. P.; Vavalle, N. A.; Rhyne, A. C.; Stitzel, J. D. (2012) Development of a full human body finite element model for blunt injury prediction utilizing a multi-modality medical imaging protocol. *12th International LS-DYNA Users Conference*, Detroit.

[7] Roth, S.; Torres, F.; Feuerstein, P.; Thoral-Pierre, K. (2013) Anthropometric dependence of the response of a thorax FE model under high speed loading: validation and real world accident replication. Computer methods and programs in biomedicine, **110** 2: 160–170.

[8] Iwamoto, M.; Nakahira, Y. (2015) Development and Validation of the Total HUman Model for Safety (THUMS) Version 5 Containing Multiple 1D Muscles for Estimating Occupant Motions with Muscle Activation During Side Impacts. Stapp car crash journal, **59**: 53–90.

[9] Untaroiu, C. D.; Pak, W.; Meng, Y.; Schap, J.; Koya, B.; Gayzik, S. (2018) A Finite Element Model of a Midsize Male for Simulating Pedestrian Accidents. Journal of biomechanical engineering, **140** 1.

[10] Grindle, D.; Pak, W. et al. (2021) A detailed finite element model of a mid-sized male for the investigation of traffic pedestrian accidents. Proceedings of the Institution of Mechanical Engineers. Part H, Journal of engineering in medicine, **235** 3: 300–313.

[11] Goumtcha, A. A.; Thoral-Pierre, K.; Roth, S. (2014) Biomechanical model of the thorax under blast loading: a three dimensional numerical study. International journal for numerical methods in biomedical engineering, **30** (12): 1667–1678.

[12] Bodo, M.; Bracq, A.; Delille, R.; Marcheal, C.; Roth, S. (2017) Thorax injury criteria assessment through non-lethal impact using an enhanced biomechanical model. Journal of Mechanics in Medicine and Biology, **17** (7): 1740027.

[13] Bracq, A.; Delille, R.; Maréchal, C.; Bourel, B.; Roth, S.; Mauzac, O. (2019) Rib fractures prediction method for kinetic energy projectile impact: from blunt ballistic experiments on SEBS gel to impact modeling on a human torso FE model. Forensic science international, **297**: 177–183.

[14] Ivanov, I.; Tabiei, A. (2004) Loosely woven fabric model with viscoelastic crimped fibres for ballistic impact simulations. International Journal for Numerical Methods in Engineering, **61** 10: 1565–1583.

[15] Shahkarami, A.; Vaziri, R. (2007) A continuum shell finite element model for impact simulation of woven fabrics. International Journal of Impact Engineering, **34** 1: 104–119.

[16] Boljen, M.; Hiermaier, S. (2012) Continuum constitutive modeling of woven fabrics. The European Physical Journal Special Topics, **206** 1: 149–161.

[17] Klein, H.; Jenerowicz, M.; Trube, N.; Boljen, M. (2020) How to Combine 3D Textile Modeling with Latest FE Human Body Models. Advances in Transdisciplinary Engineering (11): 166–177.

[18] Boljen, M.; Jenerowicz, M.; Bauer, S.; Straßburger, E. (2023) Combining protective clothes with human body models for FE ballistic impact simulations. *CDATP - Communications in Development and Assembling of Textile Products*, Berlin.

[19] Straßburger, E.; Bauer, S.; Boljen, M.; Jenerowicz, M.; Amlung, E. (2021) Innovative Schutzausrüstung mittels neuer Materialien und Auslegungsverfahren - Abschlussbericht, Fraunhofer Institute for High-Speed Dynamics, Ernst-Mach-Institut (EMI), (unpublished internal report).

[20] Clare, V. R.; Lewis, J. H.; Mickiewicz, A. P.; Sturdivan, L. M. (1975) Blunt Trauma Data Correlation, The Defense Technical Information Center (DTIC), Aberdeen Proving Ground, Maryland 21010.

[21] Sturdivan, L. M.; Viano, D. C.; Champion, H. R. (2004) Analysis of injury criteria to assess chest and abdominal injury risks in blunt and ballistic impacts. The Journal of trauma, **56** (3): 651–663.

[22] Sandler, G.; Leishman, S.; Branson, H.; Buchan, C.; Holland, A. J. A. (2010) Body wall thickness in adults and children--relevance to penetrating trauma. Injury, **41** 5: 506–509.

[23] Viano, D. C.; Lau, I. V. (1988) A viscous tolerance criterion for soft tissue injury assessment. Journal of biomechanics, **21** 5: 387–399.

[24] Bir, C.; Viano, D. C. (2004) Design and injury assessment criteria for blunt ballistic impacts. The Journal of trauma, **57** (6): 1218–1224.

[25] Bir, C.; Viano, D.; King, A. (2004) Development of biomechanical response corridors of the thorax to blunt ballistic impacts. Journal of biomechanics, **37** (1): 73–79.

[26] Agnew, A. M.; Murach, M. M. et al. (2018) Sources of Variability in Structural Bending Response of Pediatric and Adult Human Ribs in Dynamic Frontal Impacts. Stapp car crash journal, **62**: 119–192.

[27] Li, Z.; Kindig, M. W.; Subit, D.; Kent, R. W. (2010) Influence of mesh density, cortical thickness and material properties on human rib fracture prediction. Medical engineering & physics, **32** 9: 998–1008.